SOILS AND FOUNDATIONS Vol. 43, No. 4, 229–241, August 2003
Japanese Geotechnical Society

PREDICTED AND OBSERVED PERFORMANCE OF AN OIL TANK FOUNDED ON SOIL-CEMENT COLUMNS IN CLAYEY SOILS

S. RAMPELLO[i] and L. CALLISTO[ii]

ABSTRACT

In this Paper, a back-analysis of the behaviour of an oil tank during a loading test is presented, and the results of the analysis are compared with the actual performance of the tank resulting from field measurements. The tank is founded on stiff cohesive soils and on a clayey backfill improved with soil-cement columns, obtained with the deep-mixing technique. The constitutive model used in the analysis is capable to reproduce the soil non-linearity and has been calibrated using in-situ measurement of the stiffness at small strains. The backfill improved with stabilised columns is regarded as an equivalent homogenous material, characterised by a non-linear stress-strain behaviour. A coupled consolidation analysis is carried out, that provides a satisfactory simulation of the observed time-settlement curve and of the overall field of displacements monitored during the loading test. A less satisfactory agreement is obtained between measured and computed values of pore water pressure. The effectiveness of the soil improvement scheme adopted is finally evaluated, comparing the back-analysed performance with the results of additional analyses, in which no treatment or a different geometry of treatment are hypothesised.

Key words: case history, cohesive soil, deep mixing soil stabilisation, non-linear, numerical analysis, oil tank, settlement, soil improvement (**IGC**: D6/E2/H1)

INTRODUCTION

Reliable evaluation of ground movements associated with construction and/or excavation works requires a number of steps, including accurate definition of soil profile, hydraulic conditions and in-situ stress, careful geotechnical characterisation from both in-situ and laboratory tests, detailed information on project details and loading history, and appropriate description of mechanical soil behaviour. In the past 20 years it has been shown that under working load conditions soil behaviour is mainly controlled by its properties at small strain levels (0.01 to 0.1%) including high stiffness and marked stress-strain non-linearity (Jardine et al., 1986; Burland, 1989). Therefore, to predict the performance of structures, it is important to use a soil model which can account for an high initial stiffness at small strains and for a progressive decay of stiffness occurring as strains increase. Shallow foundations on soft normally consolidated clays may cause gross yield to occur, inducing large plastic strains in the foundation soils. In these cases, accurate modelling of the small-strain stiffness may not be necessary; rather, attention should be focused on the location of the gross yield surface and on the modelling of post-yield behaviour. On the contrary, when shallow foundations involve stiff clayey soils, small to medium strains are induced in the subsoil, and the description of soil non-linearity at such strain levels is essential (e.g. Burland, 1989).

In this work, a numerical simulation of the behaviour of the shallow foundation of an oil tank is presented and compared with the observed field performance. The oil tank is located at the site of Pietrafitta where the Italian State Electricity Agency (ENEL S.p.A.) has built a thermo-electrical power plant. For the soils found at Pietrafitta, a detailed geotechnical characterisation of the foundation soils is available (Rampello et al., 2002). The major engineering challenges at Pietrafitta were related to the presence of a backfill in the top 20 m, made of lumps of clay excavated from an open cast mine. This mine waste is made of an assembly of irregularly-shaped clayey blocks, resulting in a strongly heterogeneous material.

The major concern for the shallow foundations of some structures of the power plant was that of insufficient bearing capacity and excessive settlements caused by the poor mechanical properties of the mine waste. It was then decided to improve the mechanical properties of the mine waste by creating soil-cement stabilised columns with the deep-mixing technique (Calabresi et al., 1994; Rampello et al., 1994; Pane et al., 1995). An extensive field monitoring of two large oil tanks founded on the treated mine waste, performed during a leakage test, proved that the selected technique was effective in maintaining the

[i] Professor, Dipartimento di Costruzioni e Tecnologie Avamate, University of Messina, Salita Sperone 31-98166 Messina-Italy (rampello@ingegneria.unime.it).
[ii] University of Rome La Sapienza, Italy (luigi.callisto@uniroma1.it).
Manuscript was received for review on July 22, 2002.
Written discussions on this paper should be submitted before March 1, 2004 to the Japanese Geotechnical Society, Sugayama Bldg. 4F, Kanda Awaji-cho 2-23, Chiyoda-ku, Tokyo 101-0063, Japan. Upon request the closing date may be extended one month.

total and the differential settlements within the required values. A back-analysis of the settlement measured at the centre of the oil tanks during the loading test was carried out by Rampello et al. (1995) using the procedure proposed by Skempton and Bjerrum (1957) and studying consolidation under time dependent loading.

In this work, a finite element analysis of the behaviour of oil tank No. 2 is carried out, trying to model the non-linear soil behaviour at small to medium strains, relying on the data available from in-situ and laboratory testing. To this purpose, a soil model included in the model library of a commercial code is used. It is difficult to use refined soil models for the analysis of a real structure, because experimental data may not be sufficient to carry out a proper optimisation of parameters for each of the soil layers involved. Therefore, it may be interesting to evaluate the capability of a simple and readily available soil model, which is capable to capture some of the important features of soil behaviour under monotonic loading, e.g. the stress-strain non-linearity due to the development of plastic strains for small stress increments. Model calibration was carried out using test results from a cross-hole test to evaluate the small-strain shear modulus G_0 and its dependence on stress state, and results from triaxial compression tests to calibrate soil non-linearity. In the analysis, the stabilised mine waste was regarded as a homogeneous and isotropic equivalent soil characterised by non-linear behaviour as well.

SITE CHARACTERISATION AND OIL TANK DESCRIPTION

Two cylindrical oil tanks were built in the site of Pietrafitta, in Central Italy, to serve a new thermoelectrical power plant. The oil tanks, as well as the main facilities of the power plant, were to be constructed on a waste area, where the top 20–25 m of subsoil are a backfill made of clay blocks which were excavated to exploit a lignite layer from an open-cast mine. The clayey soils at Pietrafitta are of lacustrine origin. Their profile and mechanical properties are discussed extensively by Rampello et al. (2002). From the ground surface (225 m a.s.l.) downwards, the following layers are encountered:

—*S1*: clayey waste, medium to stiff, 15–25 m in thickness, with lignite fragments and thin lenses of sandy silt and ash; it is made of clayey blocks which have undergone significant swelling, weathering and softening in the time that elapsed between the excavation and the backfilling; the way it was formed resulted in a strongly heterogeneous material, characterised by an irregular net of softened surfaces;
—*S2*: lignite, 2–4 m thick, which is the unexploited lowermost portion of the original layer of brown coal;
—*S3*: peaty clay, stiff, about 5–7 m thick, with some lignite levels in the upper portion;
—*S3′*: blue silty clay, stiff, about 13 m thick;
—*S4*: clayey silt, stiff, down to a depth of 130–135 m, including layers of sandy silt and silty sand (*S5*) from 2 to 5 m thick. At the oil tank location, three main silty sand layers were identified: the first at an elevation of 175–170 m a.s.l. (z=50–55 m); the second, well recognised throughout the area, at an elevation of about 160–155 m a.s.l. (z=65–70 m); the third at an elevation of 142–137 m a.s.l.;
—sandstone bedrock, found at an elevation below 90–95 m a.s.l. (z=130–135 m).

Table 1. Physical and index properties of the foundation soils at Pietrafitta (mean values)

	γ (kN/m^3)	G_s	w (%)	W_L (%)	I_P (%)	I_L	CF (%)	A	e_0
S1	18.0	2.76	39.0	59.9	30.3	0.4	43	0.7	1.12
S2	13.1	2.25	107.0	110.4	46.1	1.0	51	1.0	2.48
S3	16.5	2.70	53.7	76.4	40.2	0.5	74	0.5	1.47
S3′	19.9	2.77	25.6	55.1	32.1	0.1	62	0.5	0.72
S4+S5	20.7	2.74	20.0	35.3	16.3	0.1	35	0.5	0.56

Average values of the physical and index properties for the different layers are reported in Table 1. The mine waste is a clayey soil of medium to high plasticity (I_P=30%) characterised by values of activity A larger than 0.5. The organic levels found in the layers *S2* and *S3* are characterised by low values of specific gravity and unit weight and by high values of water content. The silty clay (*S3′*) and the clayey silt (*S4*) are more uniform: the unit weight is nearly constant (γ=20–21 kN/m^3) while the plasticity index and clay fraction are seen to decrease gradually with depth. For these soils, the water content is close to the plastic limit, the liquidity index being close to zero.

Figure 1(a) shows the ground water head profile obtained from pore water pressure measurements in the vicinity of the oil tanks. The distribution of the ground water head H is not uniform and indicates a downward seepage from the S1, S2 and S3 soils, where H=225 m a.s.l., towards the deepest silty sand layer, where the ground water head is equal to about 207.5 m a.s.l.. Figures 1(b) and 1(c) show the profile of the overconsolidation ratio OCR and the earth pressure coefficient at rest K_0. Values of the overconsolidation ratio were obtained from oedometer test results, while K_0 values were determined using the empirical relationship with OCR and the angle of friction at constant volume φ'_{cv} proposed by Mayne and Kulhawy (1982):

$$K_0 = (1 - \sin \varphi'_{cv}) \cdot OCR^{\sin \varphi'_{cv}}. \quad (1)$$

This paper deals with the observed behaviour of oil tank No. 2, of diameter D=45 m and height H=15 m, that is located about 66 m from oil tank No. 1. Figure 2 shows a vertical section through the tank, where the details of the soil profile can be observed together with the instrumentation installed. Settlements along the perimeter of the oil tank were measured by precision levelling of 12 topographic benchmarks attached to the foundation ring beam. The deflection of the tank was also monitored using a liquid level gauge with seven measuring points. A tree-point settlement gauge E1555 was installed along the axis of the tank, measuring the rel-

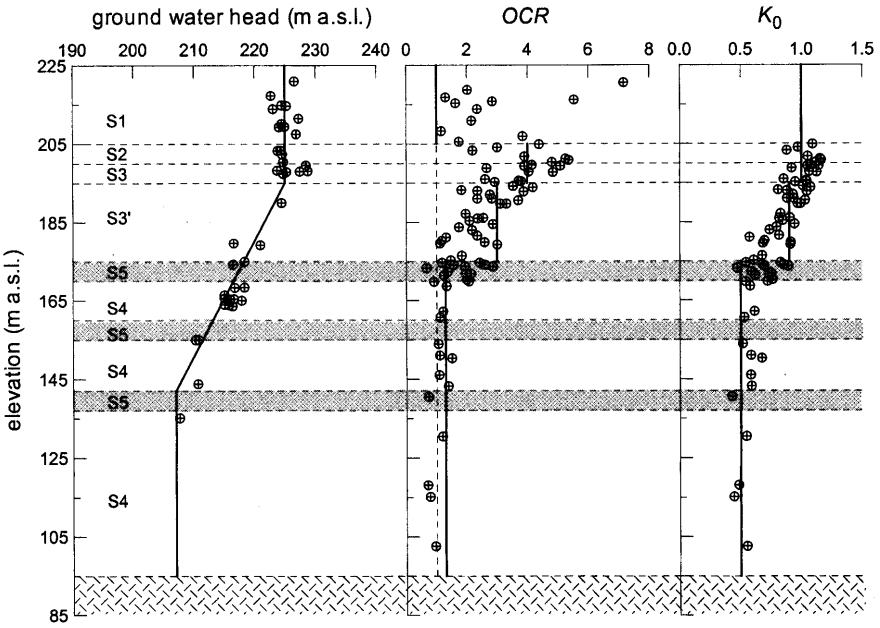

Fig. 1. Profiles of ground water head, overconsolidation ratio and earth coefficient at rest

ative vertical displacements between the ground surface and points located at the elevations of 149.5, 174.5 and 203.5 m a.s.l., the latter corresponding to the bottom of the mine waste. Inclinometers X1556 and X1391 measured the horizontal displacements along two verticals next to the perimeter of the tank. Finally, pore water pressures were measured along the axis and the perimeter of the oil tank using the strain gauged piezometers Z417A, Z1388A and Z1387AB and the Westbay multiple piezometer H319.

Since the mine waste is characterised by high compressibility and low strength, its mechanical properties were improved with stabilised columns obtained by mechanically mixing the soil with a stabilising powder agent. The stabilised soil columns were formed by firstly remoulding the soil, screwing down cutting blades attached to a drilling rig. Then, raising the blades under a reverse rotation, the stabilising agent was forced out in the soil using compressed air. A twin-head rig allowed the simultaneous installation of two columns with a diameter of 1 m and a spacing of 2 m. To improve the remoulding of the soil in the drilling stage, small quantities of water were added in the first stage of treatment. At Pietrafitta, Portland or pozzolanic 325 cement was used as stabilising agent, reacting with water in the soil during hardening and developing cemented bonding between the clay and the aggregates. A cement amount equal to 18–21% of the dry weight of soil to be treated was used. The columns are from 17 to 23 m long, reaching the lignite layer. The position of the treated columns is shown in Fig. 2. In the inner area of the tanks, the ratio of the treated area to the total area A_{col}/A is equal to about 20%, while below the foundation ring this ratio is larger and equal to about 69%.

CALIBRATION OF SOIL PARAMETERS

The behaviour of the oil tank observed during the loading test was back-analysed through a finite element coupled consolidation analysis performed using the code *Plaxis 7.2*. The mechanical behaviour of the soil was described using the constitutive model *Hardening Soil* available in the model library of the code (Schanz, 1998; Schanz et al., 1999). This is an elastic-plastic rate independent model with isotropic hardening. The elastic behaviour is defined by isotropic elasticity through a stress-dependent Young's modulus:

$$E' = E'^{\text{ref}} \left(\frac{c' \cdot \cot \varphi' + \sigma_3'}{c' \cdot \cot \varphi' + p^{\text{ref}}} \right)^m \tag{2}$$

where σ_3' is the minimum principal effective stress, c' is the cohesion, φ' is the angle of shearing resistance, $p^{\text{ref}} =$ 100 kPa is a reference pressure; E'^{ref} and m are model parameters.

The model has two yield surfaces f_s and f_v with independent isotropic hardening depending on distortional plastic strain $\gamma^p = (2 \cdot \varepsilon_1^p - \varepsilon_v^p)$ and on volumetric plastic strains ε_v^p, respectively (Fig. 3); the two surfaces have the following equations:

$$f_s = \frac{1}{E_{50}'} \frac{q}{(1 - 0.9 \cdot q/q_f)} - \frac{2q}{E'} - \gamma^p = 0 \tag{3}$$

$$f_v = \frac{\tilde{q}^2}{\alpha^2} + p'^2 - p_c'^2 = 0. \tag{4}$$

In Eq. (3), q is the deviatoric stress (*see* Eq. (13) later) and E_{50}' is given by an expression similar to Eq. (2); for plastic loading starting from an isotropic stress state, E_{50}' is equal to the secant modulus at 50% of the failure deviator stress q_f. Hardening of the f_s surface is isotropic and depends on the plastic distortional strain $\gamma^p = (2 \cdot \varepsilon_1^p - \varepsilon_v^p)$.

In Eq. (4), $p' = (\sigma_1' + \sigma_2' + \sigma_3')/3$ is the mean effective

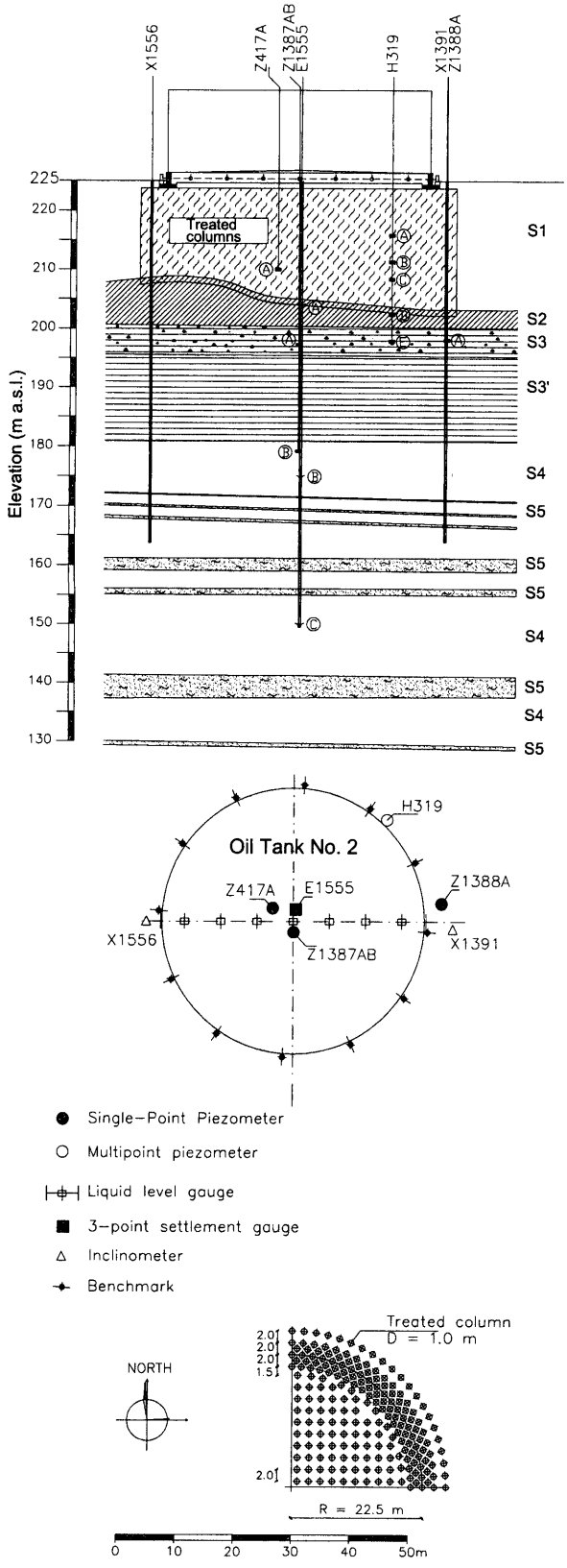

Fig. 2. Vertical section and plan view of the oil tank, indicating the position of monitoring instrumentation and soil-cement columns

stress; $\tilde{q}$ is a generalised deviator stress that accounts for the dependence of strength on the intermediate principal effective stress σ'_2; α controls the shape of the f_v surface in the $\tilde{q}-p'$ plane and can be related to the coefficient of

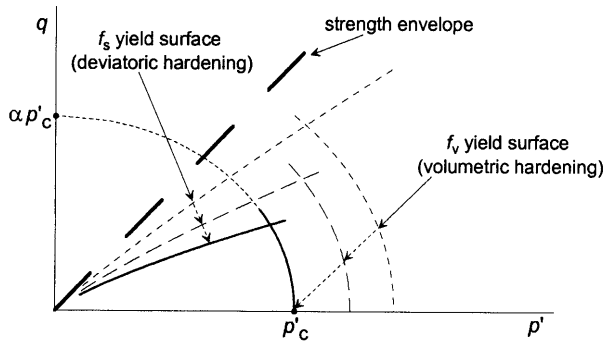

Fig. 3. Yield surfaces of the hardening soil model and their evolution

earth pressure at rest K_0 for normally consolidated states (Schanz et al., 1999). The hardening parameter p'_c is the size of the current f_v surface and is related to the plastic volumetric strains ε_v^p through the hardening law, written in the incremental form as:

$$d\varepsilon_v^p = \frac{\beta}{p^{ref}} \left(\frac{p'_c}{p^{ref}} \right)^m \cdot dp'_c \tag{5}$$

where β is a parameter that controls the variation of p'_c with the plastic volumetric strains. In the model formulation implemented in *Plaxis*, the parameter E'_{oed}, which is related to β, has to be specified. This is the constrained modulus for one-dimensional plastic loading, and depends on the maximum principal effective stress σ'_1 through the relationship:

$$E'_{oed} = E'^{ref}_{oed} \cdot \left(\frac{c' \cdot \cot \varphi' + \sigma'_1}{c' \cdot \cot \varphi' + p^{ref}} \right)^m \tag{6}$$

where σ'_1 is the maximum principal effective stress.

The initial value of the hardening parameter p'_c is related to the one-dimensional vertical yield stress, and can therefore be specified by assigning a value for the over-consolidation ratio *OCR*.

The flow rule is associated for states lying on the surface f_v, while a non-associated flow rule is used for states on the surface f_s. The latter is derived from the theory of stress dilatancy by Rowe (1962); the mobilised dilatancy angle ψ_m depends on the current stress state through the angle of mobilised friction φ'_m and the angle of friction at constant volume φ'_{cv}:

$$\sin \psi_m = \frac{\sin \varphi'_m - \sin \varphi'_{cv}}{1 - \sin \varphi'_m \sin \varphi'_{cv}} . \tag{7}$$

In turn, φ'_{cv} can be obtained from the angle of shearing resistance φ' and the angle of dilatancy ψ at failure:

$$\sin \varphi'_{cv} = \frac{\sin \varphi' - \sin \psi}{1 - \sin \varphi' \sin \psi} . \tag{8}$$

Figure 3 shows the shape of the yield surfaces f_v and f_s and schematically indicates their evolution.

For plastic loading from isotropic stress states, the model predicts an hyperbolic stress-strain relationship with tangent initial modulus equal to E'. Therefore, values of E' have been related to the shear modulus at small-strain G_0 obtained from a cross-hole test carried

out in the site, at a distance of about 200 m from the oil tanks. Figure 4 shows the profile of G_0 against the elevation a.s.l. Although the local soil profile is slightly different, it is possible to distinguish the same lithological units found below the oil tanks. The continuous line in the figure represents the prediction of G_0 obtained using Eq. (2) with the values of c', φ', E'^{ref} and m reported in Table 3. Specifically, the values of σ_3' were obtained using the profiles of ground water head and K_0 shown in Fig. 1; E'^{ref} and m were obtained by best fitting the cross-hole test results and using an average Poisson ratio $\nu'=0.2$ as obtained from drained triaxial test data. The strength parameters used in Eq. (2) are those reported by Rampello et al. (2002) for the soils found at Pietrafitta.

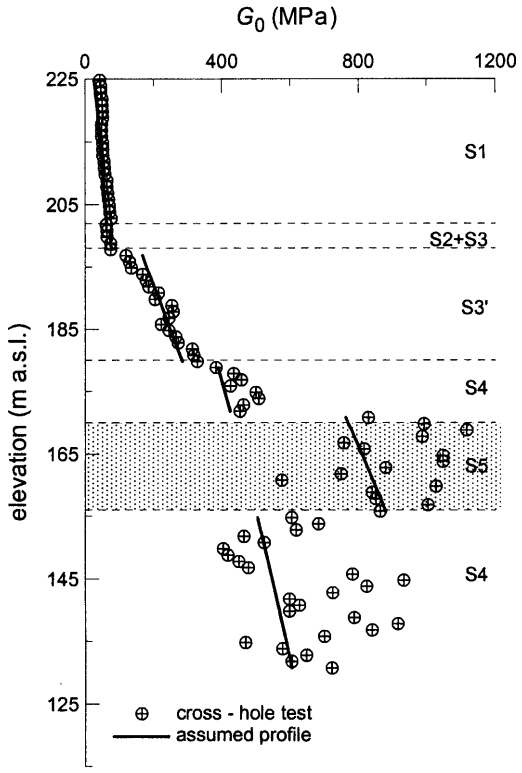

Fig. 4. Profile of the small strain shear modulus measured in a cross-hole test

Table 2. Unconfined tests on treated samples

	C_u (45 days)	C_u (90 days)
Mean (MPa)	0.68	1.07
Stand. dev. (MPa)	0.58	0.81
c.o.v. (%)	86	76
N°. of tests	30	655

The remaining model parameters $E_{50}'^{\text{ref}}$ and $E_{\text{oed}}^{\text{ref}}$ were calibrated on the results of consolidated undrained triaxial compression tests (TX-CIU) carried out on undisturbed samples retrieved with standard thin-walled open tube samples. Figure 5 shows the comparison between the model simulations and the test results obtained for the peaty clay (*S3*), the silty clay (*S3'*) and the clayey silt (*S4*). It was found that a good agreement for both the stress-strain curves and the generated excess pore water pressures can be obtained using ratios of $E'^{\text{ref}}/E_{50}'^{\text{ref}}=10$ and of $E_{\text{oed}}'^{\text{ref}}/E_{50}'^{\text{ref}}=1.2$ and a value for the angle of dilatancy at failure $\psi=0$. For the silty clay samples, the pre-failure stiffness is somewhat overestimated, although the computed excess pore water pressure match closely the experimental ones. Figure 6 shows a comparison between the $G/G_0-\varepsilon_a$ curve predicted by the model and those observed in the standard TX-CIU tests for layer *S3*. In this plot, $G=\Delta q/3\Delta\varepsilon_a$ is the equivalent secant shear modulus and ε_a is the axial strain. The diagram shows that the secant stiffness predicted by the model starts from the small-strain elastic value and, for $\varepsilon_a>0.002\%$, decreases progressively as strains increase. Since displacement of the samples was measured with external transducers, experimental data are available only for strains larger than about 0.1%; they plot closely around the curve computed with the soil model.

The portion of mine waste located underneath the oil tanks and improved with treated columns was regarded as a homogeneous soil with enhanced stiffness and strength. This choice followed the results of a preliminary analysis, in which the treated soil was modelled as a series of treated and untreated concentric cylinders, each with its own mechanical properties. It was observed that the results were approximately equivalent to those obtained using an equivalent homogenous continuum.

The small-strain stiffness of a single treated column was evaluated assuming:

$$\frac{G_{0(\text{col})}}{G_{0(\text{s})}}=\frac{C_{u(\text{col})}}{C_{u(\text{s})}} \tag{9}$$

Table 3. Soil parameters adopted in the analysis

	G_0^{ref} (MPa)	E'^{ref} (MPa)	$E_{50}'^{\text{ref}}$ (MPa)	$E_{\text{oed}}'^{\text{ref}}$ (MPa)	m	c' (kPa)	φ' (°)	OCR	K_0	k_v (m/s)
S1	70	168	16.8	20.2	0.6	10	22	1	1	$1.1\cdot10^{-9}$
$S1_{\text{t-center}}$	142	312	31.2	37.4	0.5	100	10	1	1	$5.4\cdot10^{-10}$
$S1_{\text{t-edge}}$	284	624	62.4	74.9	0.5	140	10	1	1	$5.4\cdot10^{-10}$
S2	70	168	16.8	20.2	0.6	60	15	4	1	$4\cdot10^{-8}$
S3	70	168	16.8	20.2	0.6	60	15	4	1	$4\cdot10^{-9}$
S3'	127	305	30.5	36.6	1.0	30	20	3	0.9	$7\cdot10^{-9}$
S4	243	583	58.3	70.0	0.63	44	25	1.3	0.5	$7\cdot10^{-8}$
S5	400	960	96.0	115.2	0.5	0	30	1.3	0.5	$7\cdot10^{-6}$

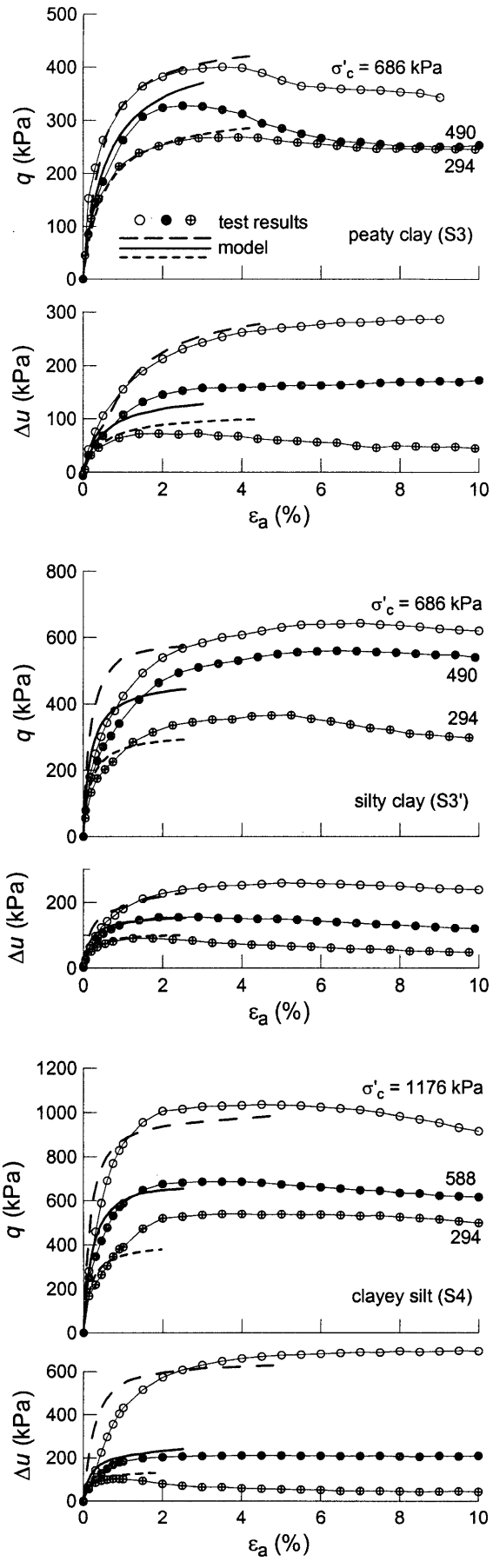

Fig. 5. Comparison between stress strain-response from TX-CIU tests and model simulations

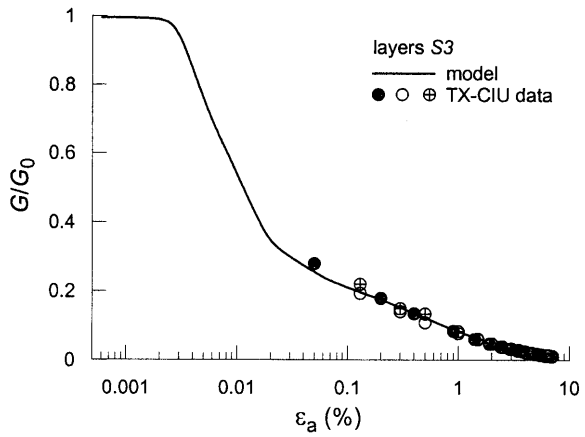

Fig. 6. Decay of secant normalised stiffness with strain predicted by the model, compared with the TX-CIU experimental data

where the undrained strength of the treated columns $C_{u(col)}$ was evaluated through unconfined compression tests on samples retrieved from about 100 columns, after curing periods of 45 and 90 days (Table 2). An average increase in strength of about 57% was observed with time. Test results indicate a strong heterogeneity of the soil treatment with values of the coefficient of variation $c.o.v. = 76$–86%. Visual inspection of stabilised pilot columns evidenced that the soil-cement mixing was not homogeneous along the columns length in that thin zones of untreated soil were observed, where the mixing had not been effective because of the presence of stiffer clays elements. A percentage as high as 27% of 249 samples retriened from the oil tank area showed values of $C_{u(col)}$ smaller than 250 kPa. Due to the scatter observed in the test results, an operational value of $C_{u(col)} = 260$ kPa was chosen from measurements after 90 days, as the average value minus the standard deviation in a normal statistical distribution. This figure is about five times larger than the mean undrained shear strength of the untreated mine waste $C_{u(s)} = 53$ kPa.

The equivalent shear modulus of the treated mine waste was obtained scaling the small-strain stiffness of the mine waste by the strengths of the treated and untreated soil, and accounting for the treated areas:

$$G_{0(eq)} = G_{0(s)}\left[1 + \left(\frac{C_{u(col)}}{C_{u(s)}} - 1\right)\frac{A_{col}}{A}\right]. \qquad (10)$$

The Young's modulus E'^{ref} of the equivalent homogeneous soil was obtained using $m = 0.5$ and $\nu' = 0.1$, which is a value typical for a cement concrete. The model parameters E'_{50} and E'_{oed} were scaled in a similar way.

The soil parameters chosen for the foundation soils are summarised in Table 3 together with the values adopted for the coefficient of earth pressure at rest K_0 and the overconsolidation ratio *OCR* (*see* Fig. 1). The strength properties of the treated soil were obtained regarding again the mine waste-columns system as a homogeneous equivalent continuum with undrained shear strength given by the relationship:

$$C_{u(eq)} = C_{u(s)}\left[1 + \left(\frac{C_{u(col)}}{C_{u(s)}} - 1\right)\cdot\frac{A_{col}}{A}\right]. \quad (11)$$

In order to use an effective stress model for the treated soil, the undrained model response was calibrated varying c' in order to obtain the observed undrained shear strength; a small value of $\varphi' = 10°$ was used as the model requires a non-zero value for φ'. This procedure yielded the values of c' and φ' reported in Table 3 for the equivalent treated mine waste.

The values of the coefficient of permeability in the vertical direction k_v were evaluated from standard incremental loading oedometer tests for the natural soils and from the back-analysis of a preliminary field loading test for the treated mine waste.

Laboratory tests are known to underestimate in-situ permeability because of scale effects related to the nature and the origin of the deposit. Therefore, higher values of k_v were adopted in the analysis, based on the results obtained for a number of case histories from back-analyses of consolidation processes in Italian clay deposits (A.G.I., 1979). For lacustrine clays, the ratio of the in-situ to the laboratory coefficient of consolidation was in the range 2–3 and the horizontal coefficient of consolidation was up to 5 times the vertical one, from both in-situ and laboratory measurements. In this study, laboratory values of k_v for the natural soil were multiplied by 3 and, for the clay layers only, the horizontal coefficient of permeability k_h was set equal to $5 \cdot k_v$. For the sandy silt layer *S5* and for the treated and untreated mine waste, which is an artificial backfill and in principle should not have any preferential direction of layering, it was assumed $k_h = k_v$.

For the treated mine waste, the coefficient of permeability was evaluated from the back-analysis of a preliminary field loading test carried out at the site of Pietrafitta (Paviani and Pagotto, 1991). The treated columns, of length $L = 16$ m and diameter $D = 1.0$ m, were located at a spacing $s = 1.5$ m, while the rectangular loading area was of 6×12 m^2. Using the solutions by Poulos and Davis (1972) for the consolidation processes under two- and three-dimensional conditions, a value of the coefficient of consolidation $c_v = 1.16 \cdot 10^{-6}$ m^2/s was calculated from the measured settlements; an estimate of $k_v \approx 4 \cdot 10^{-10}$ m/s was then obtained for the treated mine waste assuming a Young's modulus of 31.2 MPa. The layers of silty sand *S5* and of lignite *S2* were characterised by values of k_v of 1 to 2 orders of magnitude larger than those of the adjacent layers.

Starting from this set of permeability coefficients, additional adjustments were needed in order to get a satisfactory match between the predicted and the observed settlement rates of the oil tank, keeping the k_v ratios between different layers constant. The final values of k_v adopted in the analysis are listed in Table 3.

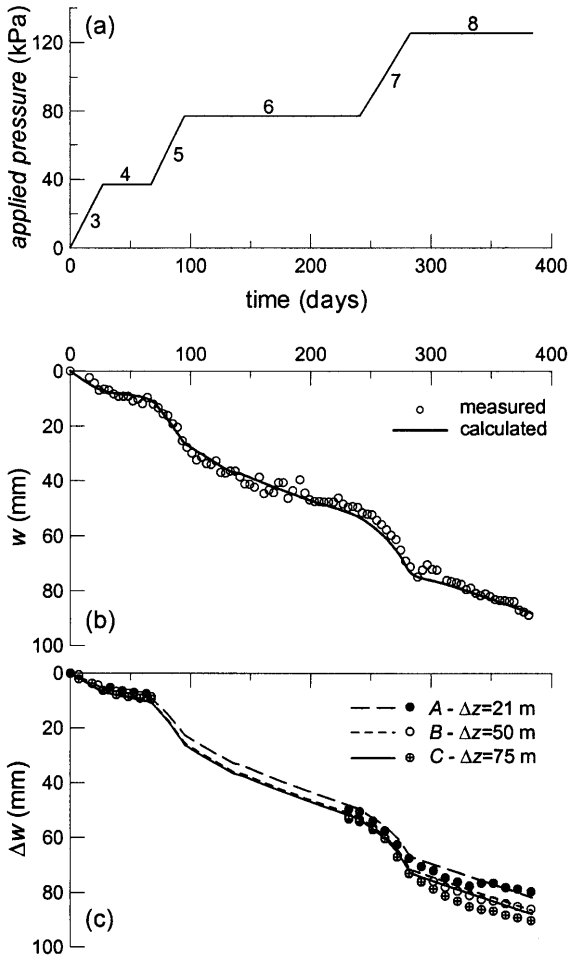

Fig. 7. Measured and calculated displacements under the centre of the oil tank: (a) loading history, (b) ground settlements and (c) relative displacements between ground surface and measuring points of settlement gauge E1555

COMPARISON OF OBSERVED AND COMPUTED BEHAVIOUR

Construction of the oil tank, corresponding to the application of a net average pressure of 37 kPa, was completed in 61 days. The leakage test was started after another 322 days: it included three loading stages up to 1/3, 2/3 and 3/3 of the tank capacity, corresponding to the application of additional average pressures of 37, 77 and 125 kPa respectively. Figure 7(a) shows the loading history of the oil tank, where time is counted from the start of the leakage test, when zero measurements for all instruments were taken.

A fully coupled finite element consolidation analysis was carried out under axisymmetric conditions. Triangular 15-noded elements were used, with a fourth-order polynomial interpolation for the displacements and a third-order interpolation for the pore water pressure, for a total of 690 elements. In the axisymmetric approximation, the contact between the mine waste and the lignite was located at the average elevation of 204.5 m a.s.l. The finite elements mesh extended horizontally to 300 m from the axis of the oil tank and vertically down to the bedrock

Table 4. Measured and computed settlements

Stage	Measured		Calculated		Measured/Calculated	
	w_{axis} (mm)	w_{edge} (mm)	w_{axis} (mm)	w_{edge} (mm)	Axis	Edge
3	5.9	2.9	7.2	2.4	0.82	1.20
4	9.5	3.7	10.8	3.3	0.88	1.11
5	27.0	9.6	27.2	8.7	0.99	1.10
6	50.0	17.9	53.4	16.8	0.94	1.07
7	74.0	22.5	73.3	22.9	1.01	0.98
8	91.0	26.5	88.2	26.8	1.03	0.99

found at 95.0 m a.s.l. Vertical sides were restrained in the horizontal direction, while displacements of the bottom of the mesh were restrained in all the directions. The initial distribution of ground water head shown in Fig. 1 was used in the analysis as a stationary condition, implying a downward seepage. The bedrock was regarded as a permeable boundary, because its upper part is heavily fractured, with a constant ground water head equal to 207 m a.s.l. The sides of the mesh were assumed to be impermeable. Consolidation analyses with constant rate of loading were carried out for stages 3, 5 and 7, while consolidation analyses at constant load were carried out for stages 4, 6 and 8.

The construction of the tank was simulated first, gradually increasing a uniform pressure applied by the tank on the upper boundary of the mesh. After this stage, the computed settlement at the centre of the tank was equal to 6.5 mm. A consolidation stage of 322 days with constant load was then carried out; after this period, the consolidation process was nearly completed, the maximum excess pore pressure being smaller than 20% of the applied load. This provided an additional settlement of 11.5 mm at the centre of the tank. Subsequently, the displacements of all nodes were zeroed and the analysis was continued using the loading diagram of Fig. 7(a).

In Fig. 7(b) the settlements measured at the centre of the tank using the liquid level gauge and the precision levelling are compared with those calculated in the analysis. Measurements and calculations show a satisfactory agreement for all the loading stages. Values of the settlements measured and calculated at the centre and at the edge of the tank are reported in Table 4; ratios of the measured to the calculated settlements are in the range 0.8 to 1.2, the larger difference being obtained after the first loading stage.

Figure 7(c) shows the observed relative displacements between the ground surface and the measuring points of the settlement gauge E1555, compared with the analysis results. Measuring point A is located at the bottom of the mine waste (203.5 m a.s.l.), while points B and C are located at elevations of 174.5 and 149.5 m a.s.l. (*see* Fig. 2). Data are not available for the second loading stage, due to problems which occurred in the data logging. Therefore, to compare measurements and calculations for the third loading stage, measurements were equated to calculations at the end of stage 6. The relative displacements are almost identical, showing that most of

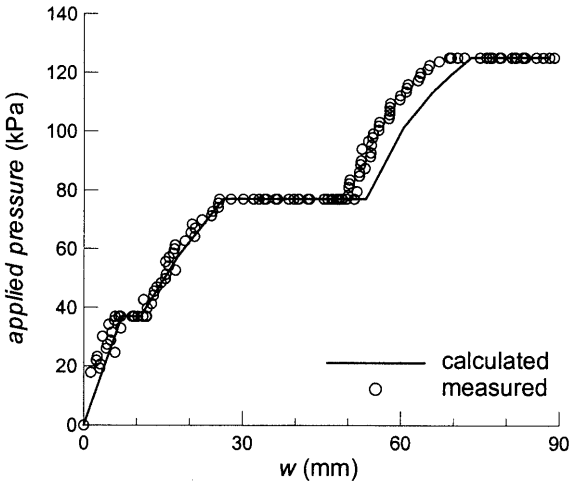

Fig. 8. Observed and computed relationship between applied pressure and settlement under the centre of the oil tank

the settlements are due to the compression of the treated mine waste. Again, a good agreement is observed between measured and computed relative displacements.

The relationship between the applied pressure and the settlements measured at the centre of the tank is compared with the computation results in Fig. 8, where the combined effect of consolidation and non-linear soil behaviour can be observed. Consolidation produces an increase of stiffness with time: the slope of the load-settlement curve at the beginning of each loading stage is larger than that observed at the end of the previous loading stage. Conversely, along a single load increment non-linear soil behaviour produces a gradual reduction in the slope of the load-settlement curve.

The settlement profiles measured with the liquid level gauge and the precision levelling are compared with the computed settlements in Fig. 9, where the distance x from the centre of the tank is divided by the radius R of the tank. A good agreement is observed for all the loading and the consolidation stages; the measured ratio of the axis to the average edge settlements is from 2.0 to 3.4, while the computed one ranges between 3.0 and 3.3. The higher density of the soil treatment close to the edge of the oil tank ($x/R=0.9$–1.1) resulted in low and uniform settlements of the foundation ring beam. Figure 10(a) shows, for stages 4, 6 and 8, the measured settlements of the benchmarks installed in the ring beam together with those of the best fit plane of rigid rotation; the maximum settlement did not exceed 30 mm, while the maximum differential settlement Δw associated with the best fit plane is lower than 3 mm (Fig. 10(b)).

The profiles of horizontal displacements measured with inclinometers X1391 and X1556 are compared with the analysis results in Fig. 11: measured and computed profiles have comparable shapes with maximum values of the horizontal displacement attained at an elevation of about 218 m a.s.l., and with displacements smaller than about 4 mm occurring below the mine waste. However, values of computed displacements are from 1.5 to about 2 times

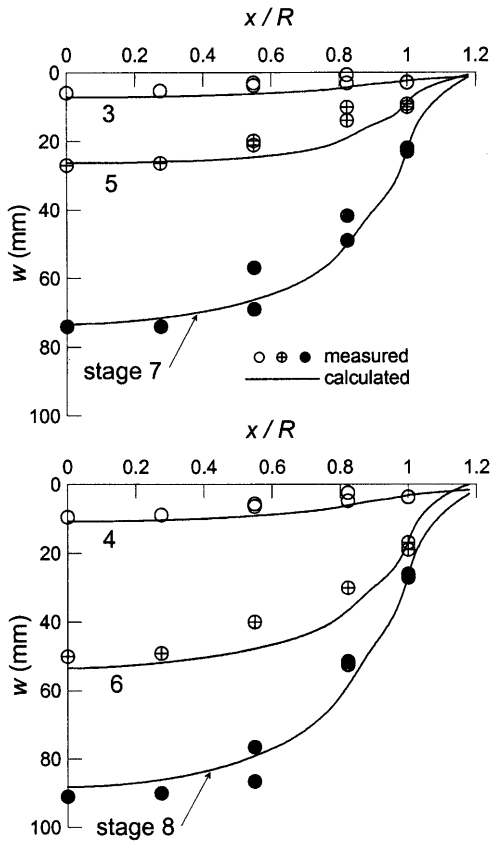

Fig. 9. Observed and computed settlement profile of the oil tank foundation

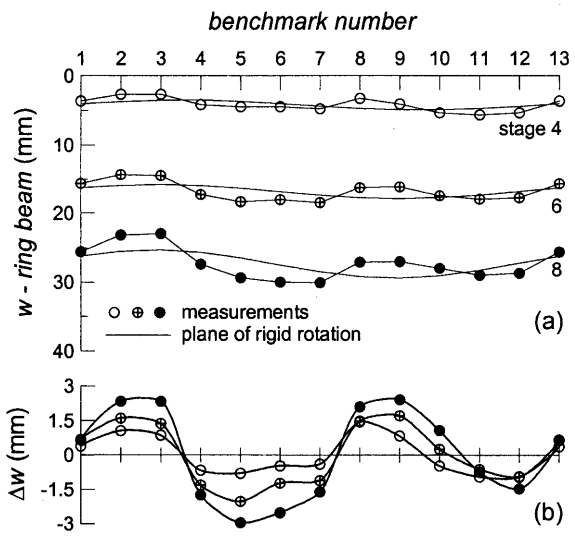

Fig. 10. Total and differential settlement of benchmarks along the foundation ring beam

larger than those measured within the mine waste.

Figure 12(a) shows the contours of equal deviatoric strain

$$\varepsilon_s = \frac{\sqrt{2}}{3}\left[(\varepsilon_r - \varepsilon_z)^2 + \varepsilon_r^2 + \varepsilon_z^2 + \frac{3}{2}\varepsilon_{rz}^2\right]^{1/2} \quad (12)$$

where subscripts r and z are for the radial and the vertical directions respectively. Contours are plotted for stage 7,

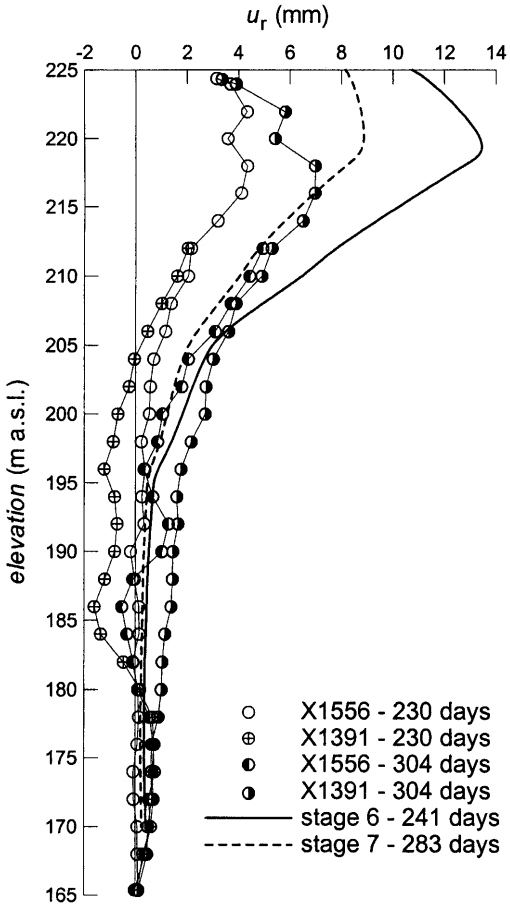

Fig. 11. Observed and computed horizontal displacements at the edge of the oil tank

at the end of the last loading step: deviatoric strains in the treated mine waste range between 0.1 and 0.4%, while most of the soil undergoes strains smaller than 0.05%. Figure 12(b) shows the contours of equal volumetric strain ε_v at the end of stage 8: small volumetric strains are obtained with values lower than 0.05% in most of the foundation soil, while values of ε_v in between 0.1 and 0.3% are calculated in the treated mine waste.

Comparison of computed and observed pore water pressures was made difficult by the malfunctioning of a significant part of the instrumentation installed; therefore, only a limited set of pore water pressure measurements may be compared with the calculation results. The excess pore water pressure Δu measured during the loading test are plotted in Fig. 13: piezometers Z417A and Z1387A are located under the axis of the oil tank, in the mine waste and in the peaty clay, at depths $z = 14.5$ and 27 m, while piezometers H319 C-D-E are located under the edge, in the mine waste ($z = 16$ m), the lignite ($z =$ 22 m) and the peaty clay ($z = 26.5$ m) (*see* Fig. 2). In the loading stages 3, 5 and 7 maximum values of measured Δu are equal to 27%, 23% and 16% of the average applied pressure, respectively. During stage 6, in which load was maintained constant for a period of 146 days, 40 to 60% of the excess pore water pressure dissipated depending on the position of the measuring cell.

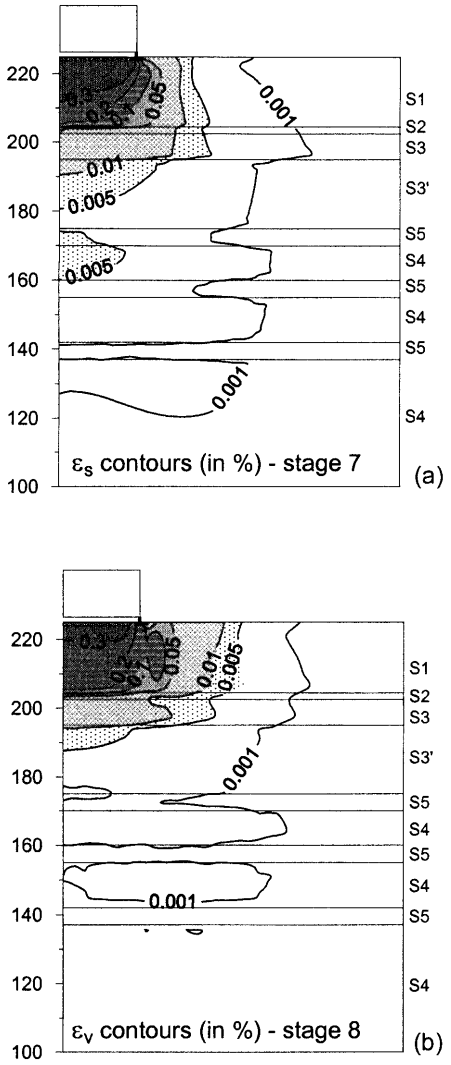

Fig. 12. Computed contours of equal shear strain (a) and volumetric strain (b)

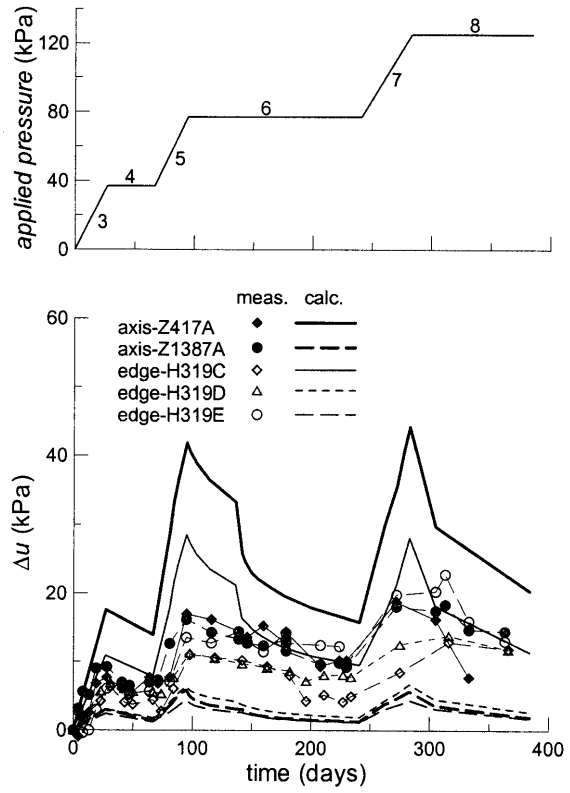

Fig. 13. Measured and calculated values of excess pore water pressure

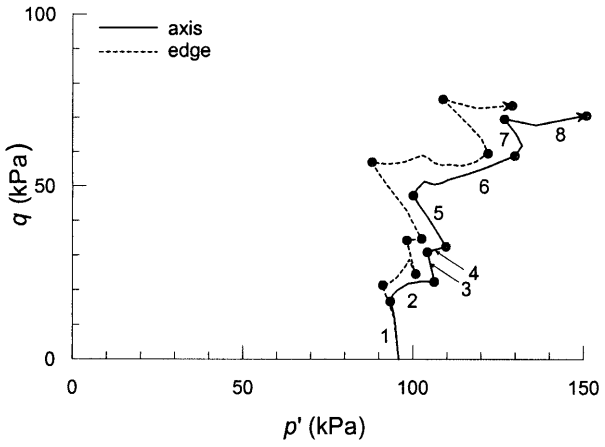

Fig. 14. Computed stress paths for soil elements located below the centre and the edge of the oil tank

The values of Δu computed at the same location of the piezometers are also plotted in Fig. 13. Higher values of Δu are calculated in the treated mine waste; specifically, maximum values of Δu of about 48%, 55% and 36% of the applied load are obtained at the end of the loading stages 3, 5 and 7, respectively. It should be noted that piezometers measured the excess pore water pressure in the untreated soil between the columns, while the computed values of Δu are relative to an ideal continuous equivalent improved soil; in order to get a consistent comparison, the computed values should be scaled by the ratio of the stiffness of the untreated soil to that of the equivalent treated mine waste, which already accounts for the density of the treatment (Eq. (10)). The ratios of initial stiffness adopted for the untreated and the equivalent soil would result in measured excess pore water pressures equal to 54% of the calculated ones under the centre and to 27% under the edge of the oil tank. However, this figures may be somewhat modified by the non-linear stress-strain response assumed for the soil.

According to the assumptions made in the analysis, low excess pore water pressures are calculated close to the high permeability lignite layer, while measurements provide higher values. During stage 6, the computed dissipation rate is higher than the experimental one in that about 60% of the excess pore water pressure is dissipated.

Figure 14 shows the stress paths for soil elements located at mid height in the treated mine waste (215 m a.s.l.), under the axis and under the edge of the tank. The stress paths are plotted in terms of the mean effective stress p' and the deviator stress q defined as:

$$q = \frac{1}{\sqrt{2}} [(\sigma'_r - \sigma'_z)^2 + (\sigma'_z - \sigma'_\theta)^2 + (\sigma'_\theta - \sigma'_r)^2 + 6\tau^2_{rz}]^{1/2} \quad (13)$$

where subscript θ indicates the tangential direction in the axisymmetric geometry.

The construction stages 1 and 2, relative to the oil tank construction, are included in the figure. For the loading stages 1, 3, 5 and 7, increase in the deviator stress is generally larger than the corresponding decrease in mean effective stress; however, the decrease in p' becomes more important as the mobilised strength increases, resulting in stress paths veering to the left. The dissipation of positive excess pore water pressure in stages 2, 4, 6 and 8 implies an increase in the mean effective stress at nearly constant values of q. Slightly higher values of deviator stress are computed below the edge of the oil tank, while larger mean effective stress are induced below the axis.

DISCUSSION AND CONCLUSIONS

The oil tank examined in this paper is founded on a clayey mine waste improved with stabilised columns, and on medium to stiff cohesive soils. Therefore, it could be anticipated that the soil would not undergo large volumetric strains, and gross volumetric yielding was not of major concern, as for similar structures founded on soft soils (Burland, 1969; Muir Wood, 1980). Rather, accurate definition of pre-failure stress-strain relationships at small to medium strains was of great importance for a reliable estimate of the performance of the tank under working load conditions. To this purpose, a constitutive model available in a commercial code was used, which is nonetheless capable of reproducing soil non-linearity due to the occurrence of plastic strains from the beginning of the loading process. The model also accounts for the dependency of stiffness on the effective stress state.

Calibration of the constitutive model was carried out using results from a cross-hole test and from standard consolidated-undrained triaxial compression tests. The cross-hole test was used to evaluate the shear modulus at small strains G_0 for each soil layer and to describe its variation with effective stress. The remaining model parameters were selected to obtain a satisfactory description of the soil non-linearity observed in the triaxial tests. The treated mine waste was regarded as a homogenous equivalent continuum, scaling the strength and stiffness parameters by a factor based on the ratios $C_{u(col)}/C_{u(s)}$ and A_{col}/A_s (Eqs. (10) and (11)).

A fully coupled consolidation analysis was carried out under axisymmetric conditions, accounting for the actual time-load sequence. Having defined the soil stiffness, consolidation response depends on the coefficient of permeability adopted. Laboratory values of the permeability coefficient measured for the natural soils had to be increased to reproduce the observed response; however, the ratio of the field to the laboratory permeability was consistent with field observations carried out in a number of Italian clayey soils of the same origin.

A good agreement was obtained between the observed and computed time-settlement curves relative to the centre of the oil tank. In addition, a satisfactory match

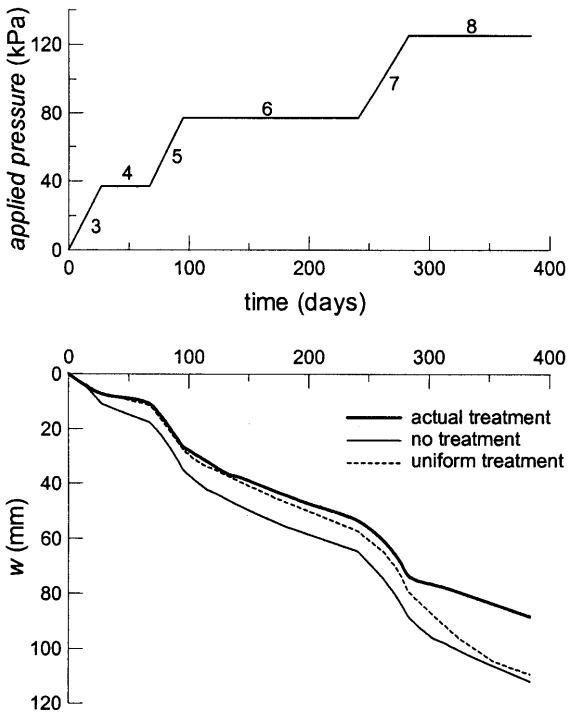

Fig. 15. Settlements at the centre of the oil tank calculated under different hypotheses for soil stabilisation

was observed for the whole displacement field, including the settlement profile of the foundation, the distribution of settlements with depth and the profile of the horizontal displacements at the edge of the tank. This validated the basic assumptions made for the pre-failure behaviour of the different layers. In fact, while the same foundation settlement could be obtained using different combinations of stiffness and permeability parameters, it is likely that just a limited set of parameters may also provide a good match for the overall distribution of displacements. For instance, computations were consistent with the observation that the settlement of the tank is mostly due to the compression of the treated mine waste. This result is related to the use of high stiffness at small strains for the natural soils, producing a rapid decrease of settlement with depth (Jardine et al., 1986). Consistently, strains computed below the mine waste are smaller than 0.05%. The effect of a high initial stiffness is also to concentrate the settlements in a limited distance around the loaded area, as shown in Fig. 9.

Only half the installed piezometers appeared to provide reliable measurements. The excess pore water pressure measured at the end of each loading stage in the treated mine waste, at a depth of about 15 m, was about 50% lower than the computed values. This is to be related to the discrepancy between the assumption of an equivalent homogeneous treated soil and the actual geometry of the stabilised mine waste. In fact, excess pore water pressures were measured between the soil-cement columns, while it can be assumed that a larger part of the applied load is transferred to the column. The ratios of the stiffness values and of the treated areas adopted for the treated

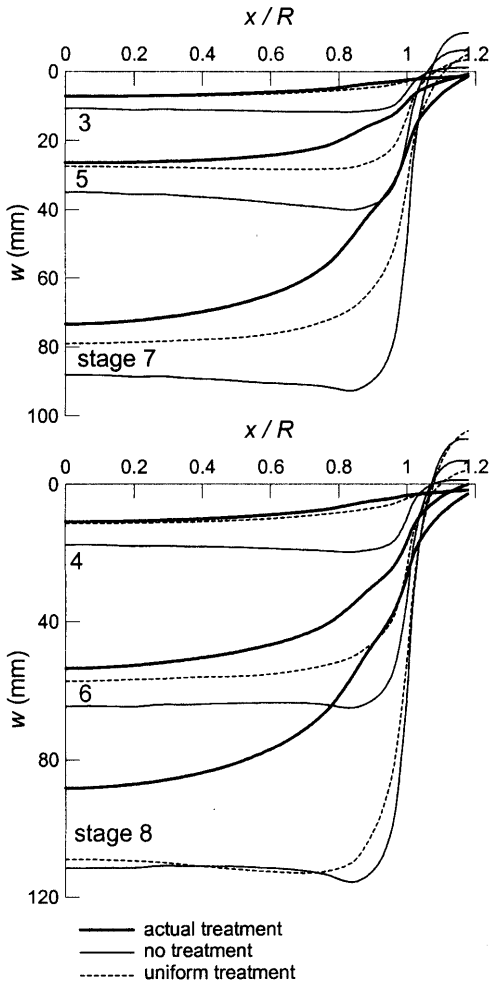

Fig. 16. Settlement profile of the oil tank calculated under different hypotheses for soil stabilisation

and untreated mine waste is roughly consistent with the obtained overestimation of Δu.

The satisfactory match between calculations and observations also shows that it is reasonable to regard the treated mine waste as a continuous equivalent material. The effectiveness of the soil stabilisation performed in the mine waste was evaluated by carrying out two additional analyses, in which the properties of the treatment were modified. Specifically, one analysis was carried out leaving unchanged the original properties of the mine waste below the tank, while in a second analysis the hypothesis was made that the column spacing was uniform and equal to that actually adopted below the inner portion of the tank ($A_{col}/A = 0.2$). The obtained time-settlement curves are compared in Fig. 15 with that computed for the actual treatment, while Fig. 16 shows the deflections computed along the diameter of the oil tank. Without soil stabilisation, settlements up to 30% larger are obtained under the axis, while a much more significant increase is obtained below the edge of the tank. Inspection of the computed stress state in the soil shows that this is due to local failure beneath the edge. Such a local failure would have probably occurred without the treatment and has been prevented by the soil stabilisation adopted.

For the case of uniform treatment, the time-settlement curve is initially similar to that computed for the actual treatment. However, starting from the last load increment the settlements at the axis become larger, approaching that relative to the case of untreated soil. In this case, as the load level increases the deviatoric stress components in the soil become important causing additional movements below the edge of the tank, though the soil does not actually reach local failure because of the enhanced strength provided by the treatment. Therefore, it seems that the design choice of using a higher density of stabilised columns below the foundation ring beam was effective in improving the overall behaviour of the oil tank, as it contributed to sustaining the increments in deviatoric stress occurring in the foundation soil below the perimeter of the oil tank.

REFERENCES

1) A. G. I. (1979): Experiences on the time-settlement behaviour of some Italian soft clays, *Proc. VII ECSMFE*, Brighton, **1**, 1-11.
2) Burland, J. B. (1969): Deformation of soft clay beneath loaded areas, *Proc. of VII ICSMFE*, Mexico City, **1**, 55-63.
3) Burland, J. B. (1989): Ninth Laurits Bjerrum Memorial Lecture: "Small is beautiful"—the stiffness of soils at small strains, *Can. Geotech. J.*, **26**, 499-516.
4) Calabresi, G., Pane, V., Rampello, S. and Bianco, O. (1994): Geotechnical problems in construction over a thick layer of a mine waste, *Proc. First Int. Congr. on Environmental Geotechnics*, Edmonton, (1) 449-454.
5) Jardine, R. J., Potts, D. M., Fourie, A. B. and Burland, J. B. (1986): Studies of the influence of non-linear stress-strain characteristics in soil-structure interaction, *Géotechnique*, **36**, (3), 377-396.
6) Mayne, P. W. and Kulhawy, F. H. (1982): $K_0 - OCR$ relationships in soil, *J. of the Geotech. Engrg. Division*, ASCE, **108**, (GT6), 851-872.
7) Muir Wood, D. (1980): Yielding in soft clay at Bäckebol, Sweden, *Géotechnique*, **30**(1), 49-65.
8) Pane, V., Rampello, S., Calabresi, G., Barluzzi, M. and Bianco, O. (1995): Caratterizzazione geotecnica di trattamenti colonnari eseguiti su discariche minerarie argillose, *Proc. XIX Conv. Naz. di Geotecnica*, A.G.I., Pavia, (1), 403-412.
9) Paviani, A. and Pagotto, G. (1991): New technological developments in soil consolidation by means of mechanical mixing, implemented in Italy for the ENEL power plan at Petrafitta, *Proc. X ECSMFE*, Florence, **2**, 511-516.
10) Poulos, H. G. and Davis, E. H. (1972): Rate of settlement under two- and three-dimensional conditions, *Géotechnique*, **7**(1), 95-114.
11) Rampello, S., Calabresi, G., Pane, V. and Bianco, O. (1995): Analisi del comportamento di due serbatoi per olio combustibile fondati su trattamenti colonnari in terreni coesivi, *Proc. XIX Conv. Naz. di Geotecnica*, A.G.I., Pavia, (1), 423-434.
12) Rampello, S., Pane, V., Calabresi, G. and Bianco, O. (1994): Geotechnical characterisation of a clayey mine waste, *Proc. First Int. Congr. on Environmental Geotechnics*, Edmonton, (1), 531-537.
13) Rampello, S., Calabresi, G. and Callisto, L. (2002): Characterisation and engineering properties of a stiff clay deposit, *Proc. of Int. Workshop on Characterisation and Eng. Properties of Natural Soils* (ed. by Tan et al.), Singapore, Swets and Zeitlinger, Lisse, **2**, 1021-1045.
14) Rowe, P. W. (1962): The stress-dilatancy relation for static equilibrium of an assembly of particles in contact, *Proc. Royal Society*, London, (A269), 500-527.
15) Schanz, T. (1998): *Zur Modellierung desMechanischen Verhaltens von Reisbungmaterialen, Habilitation*, Stuttgart Univerität.

16) Schanz, T., Vermeer, P. A. and Bonnier, P. G. (1999): Formulation and verification of the Hardening-Soil Model, *R.B.J. Brinkgreve, Beyond 2000 in Computational Geotechnics*, Balkema, Rotterdam, 281–290.

17) Skempton, A. W. and Bjerrum, L. (1957): A contribution to the settlement analysis of foundations on clay, *Géotechnique*, **7**(4), 168–178.